Journal of Materials Chemistry A

Accepted Manuscript

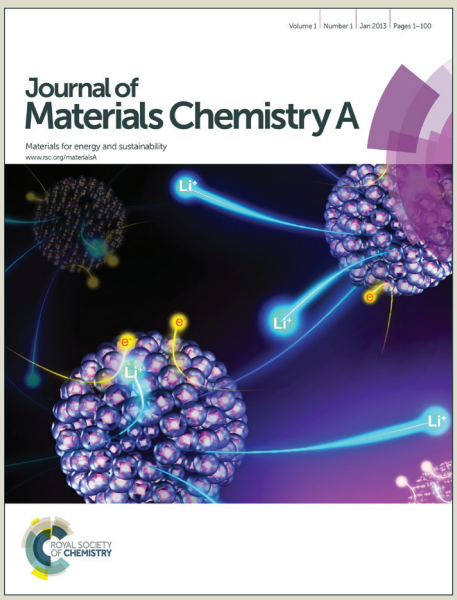

ROYAL SOCIETY OF CHEMISTRY

www.rsc.org/materialsA

Cite this: DOI: 10.1039/c0xx00000x

www.rsc.org/xxxxxx

ARTICLE TYPE

$MnMoO_4$•$4H_2O$ Nanoplates Grown on a Ni Foam Substrate for Excellent Electrochemical Properties

Yunjiu Cao,[ab] Wenyao Li,[ab] Kaibing Xu,[a] Yuxin Zhang,[a] Tao Ji,[ab] Rujia Zou,[a] Jianmao Yang,*[a] Zongyi Qin*[a] and Junqing Hu*[a]

Received (in XXX, XXX) Xth XXXXXXXXX 20XX, Accepted Xth XXXXXXXXX 20XX
DOI: 10.1039/b000000x

$MnMoO_4$•$4H_2O$ nanoplates (NPs) grown directly on Ni foam were synthesized by a facile hydrothermal process. As-grown $MnMoO_4$•$4H_2O$ NPs supported on Ni foam directly as integrated electrodes for electrochemical capacitors demonstrated prominent electrochemical performances with a high specific capacitance of 1.15 F cm^{-2} （2300 F g^{-1}） at a current density of 4 mA cm^{-2} and a good cycling ability (92% of the initial specific capacitance remained after 3000 cycles). The superior electrochemical performances could be ascribed to the porous structure of interconnected $MnMoO_4$•$4H_2O$ NPs directly grown on current collectors improving electrolyte diffusion efficiency and increasing electron transport. These $MnMoO_4$•$4H_2O$ NPs on Ni foam with remarkable electrochemical properties could be considered as a prospective electrode material for the application of supercapacitors.

1. Introduction

In the process of looking for clean energy to satisfy the growing demand for energy, ongoing research efforts have been devoted to the study of supercapacitors due to the desirable abilities, such as rapid charging, high power density, and long cycle life.[1-3] According to different ways of the storage charge, supercapacitors can be divided into two types, i.e., electric double layer capacitors storing electrical energy via reversible ionabsorption at electrode/electrolyte interface and pseudocapacitors based on fast and reversible surface redox reactions.[4,5] Supercapacitors using transition metal oxides as electrode can provide higher energy densities in comparison to the energy density delivered by the electrical double layer capacitors with carbon-based active materials as electrodes.[6,7] Therefore, transition metal oxides as electrode materials have been deemed to one of the most promising electrode materials for supercapacitors. Numerous studies on binary transition metal oxides using for electrode materials have been widely explored and developed such as MnO_2[8,9], NiO[10,11], Co_3O_4[12], and MoO_3[13]. However, the low electrical conductivity of the binary metal oxides reducing the electrode materials of electrochemical performance is a huge obstacle in the process of further application. Single-phase ternary transition metal oxides with two different metal cations, rather than mixtures of two binary metal oxides are emerging as promising electrode materials and demonstrate better electrical conductivity and better performance for electrochemical capacitors owing to the relatively low activation energy for electron transfer between cations.[14-19] Accordingly, much attention has been paid on choosing suitable ternary metal oxides materials with an appropriate structure to achieve better performance. For example, Xia et al. achieved the specific capacitance of 72 F g^{-1} at 1 mV s^{-1} scan rate for pure $CoMoO_4$.[20] Wang et al. reported superior specific capacitance of 1650 F g^{-1} at a current density of 1 A g^{-1} for $NiCo_2O_4$ urchins.[21] At present, the design and fabrication of novel ternary transition metal oxides with high electron conductivity and good electrochemical properties are still a research hotspot.[22-24]

Particularly, ternary manganese molybdenum ($MnMoO_4$) as a potential electrode material due to low cost, low toxicity, and natural abundance, recently has attracted much research interest. $MnMoO_4$ combines the contributions from both manganese and molybdenum ions offers richer redox chemistry reactions than the two single component oxides, manganese oxide and molybdenum oxide. Purushothaman and co-workers obtained a maximum specific capacitance of 998 F g^{-1} for α-$MnMoO_4$ nanorods at a scan rate of 5 mV s^{-1} in H_2SO_4 electrolyte.[25] In addition, Mai et al. reported a specific capacitance of 9.7 F g^{-1} and an energy density of 8.8 Wh kg^{-1} for the $MnMoO_4$ nanorods at a current density of 1 A g^{-1}.[26] Unfortunately, $MnMoO_4$-based materials usually adopt traditional slurry coating technique,[27] where binder-contained electroactive materials provide poor electron conductivity and only the surface part of electroactive materials in good contact with the electrolyte to participate in the Faradaic reactions for energy storage can effectively contribute to the total capacitance, leading to a less satisfactory specific capacitance. The poor electron conductivity and low specific capacitance are obstacles for the supercapacitor practical applications using these $MnMoO_4$-based materials. So, it is still a great challenge to synthesize a $MnMoO_4$ nanomaterial with large specific area and

high electrical conductivity for supercapacitor applications. One effective method is to directly grow ternary metal oxides active materials at a nanometer scale on conducting substrates as binder-free electrodes for supercapacitors. For instance, Guo et al. reported $CoMoO_4$ nanoplate arrays grown directly on Ni foam exhibited remarkable electrochemical performance with a high specific capacitance of 1.26 F cm^{-2} at a charge and discharge current density of 4 mA cm^{-2} with an excellent cycling ability (79.5% of the initial specific capacitance remained after 4000 cycles).[28] In general, directly growing ordered nanostructure on porous conductive substrates offers remarkable advantages, such as simplification of the electrode processing, availability of electrode–electrolyte contact area, faster electron diffusion, better conductivity of the active materials with substrates, higher rate capability, and sufficient Faraday reaction on the surface of individual nanostructures.[29-31]

In our study, we have designed and fabricated $MnMoO_4$•$4H_2O$ NPs on Ni foam by a facile hydrothermal route, which is directly used as a binder-free electrode for electrochemical evaluation. The as-prepared $MnMoO_4$•$4H_2O$ NPs on Ni foam applied in supercapacitors achieve better electrical conductivity because of the porous structure of the continuously porous Ni and $MnMoO_4$•$4H_2O$ NPs network with more surface area for easy diffusion of the electrolyte into the inner interface of the electrode materials and the nanomaterials on Ni foam with robust adhesion providing fast electron-transport access to the current collector, efficiently reducing Ohmic polarization, the high rate capability and better cycling stability during long-term cycling due to the NPs tightly bonding on Ni foam, building a stable mechanical structure and facilitating the electron transmission. Based on the aforementioned merits, the as-obtained Ni foam supported $MnMoO_4$•$4H_2O$ NPs exhibit a high area specific capacitance (ASC) of 1.15 F cm^{-2} (2300 F g^{-1}) at 4 mA cm^{-2} and a good cycling stability of 92% of the initial specific capacitance after 3000 cycles. These researches reveal the $MnMoO_4$•$4H_2O$ NPs is a promising electrode material in development of high performance supercapacitors.

2. Experimental Section

2.1 Synthesis of $MnMoO_4$•$4H_2O$ NPs on Ni foam

All solvents and chemicals used in the experiment were of analytical grade and used without further purification. Manganese chloride and sodium molybdate were obtained from Sinopharm. $MnMoO_4$•$4H_2O$ NPs were synthesized via a facile hydrothermal method. Prior to the synthesis, a piece of Ni foam substrate was washed with 6M HCl aqueous solution in an ultrasound bath for 25 min to remove the NiO layer on the surface, and rinsed with deionized water and absolute ethanol several times. Then the reaction solution was obtained by mixing 2 mmol $MnCl_2$•$4H_2O$ and 2 mmol Na_2MoO_4•$2H_2O$ in 40 mL distilled water under constant magnetic stirring. After being stirred for 1h, as-prepared solution then was transferred into a 50 mL Teon-lined stainless steel autoclave liner. The washed Ni foam substrate was immersed in the reaction solution and placed standing against the wall of a Teon-lined autoclave. The liner was sealed in a stainless steel autoclave and maintained at 150 °C for 8 hours in an electric oven. After the autoclave was cooled down to room temperature naturally, the sample on the Ni foam was carefully cleaned with deionized water and absolute ethanol with the assistance of ultrasonication. Then the Ni foam with products was placed in drying oven at 60 °C overnight. The $MnMoO_4$•$4H_2O$ powders were synthesized as the same hydrothermal conditions as the $MnMoO_4$•$4H_2O$ NPs on Ni foam. (for details, part 1, see ESI†) The mass loading of the $MnMoO_4$•$4H_2O$ NPs on Ni foam and the $MnMoO_4$•$4H_2O$ powders was calculated to be about 0.5 and 1.7 mg cm^{-2}, respectively. (for details, Part 1, see ESI†)

2.2 Materials characterization

The synthesized samples were characterized with a D/max-2550 PC X-ray diffractometer (XRD; Rigaku, Cu-Kα radiation) and X-ray photoelectron spectroscopy (XPS, PHI5000VersaProbe), the morphology and microstructure of electrode materials were characterized using a scanning electron microscopy (SEM; S-4800) and a transmission electron microscopy (TEM; JEM-2100F) equipped with an energy dispersive spectrometer (EDS). The mass of electrode materials was weighed on a XS analytical balance (Mettler Toledo; δ = 0.01 mg).

2.3 Electrochemical Characterizations

Electrochemical performances were examined on an Autolab (PGSTAT302N potentiostat) with a three-electrode mode. The reference electrode and counter electrode were saturated calomel electrode(SCE) and platinum, respectively. The 1M NaOH aqueous solution was used as electrolyte. The Ni foam-supported nanostructures of $MnMoO_4$•$4H_2O$ electrode materials acted directly as the working electrode.

3. Results and Discussion

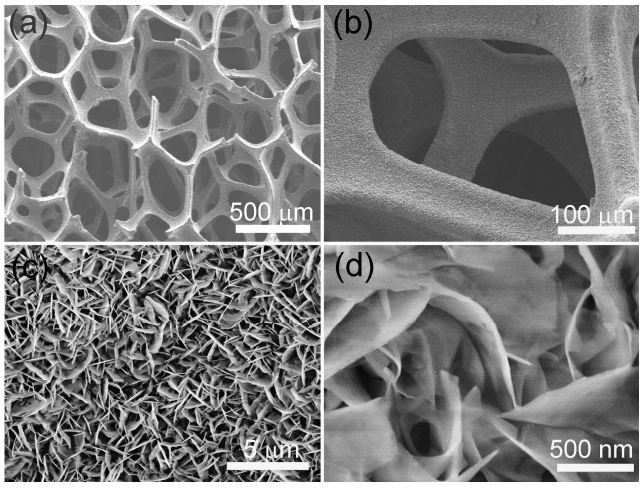

Fig. 1 (a) The 3D structure of bare Ni foam. (b-d) low and high magnification SEM images of $MnMoO_4$•$4H_2O$ NPs grown directly on Ni foam.

The morphology and microstructure of the $MnMoO_4$•$4H_2O$ NPs on Ni foam are shown in Fig. 1. Fig. 1(a) shows a low-magnification scanning electron microscopy image of a bare net-like Ni foam with 3D porous structure after treatment with a HCl solution. 3D Ni foam was employed as the current collector due to its large and uniform macropores structure, large supporting area, and high electrical conductivity. Most importantly, the Ni

foam with 3D structure can provide efficient and rapid pathways with ion and electron transport for electrode materials. The low-magnification SEM image in Fig. 1(b) reveals $MnMoO_4$•$4H_2O$ NPs grown uniformly covering the whole Ni foam. As can be seen from Fig. 1(c) of the SEM image, as-grown products on Ni foam are distinctly interconnected with each other and make up an ordered structure with an opened-up network. So as an electrode for supercapacitors, they can provide a huge surface area in contact with the electrolyte. Fig. 1(d) is a higher magnification SEM image, where the average thickness of a single $MnMoO_4$•$4H_2O$ nanoplate is estimated to be about 10 nm.

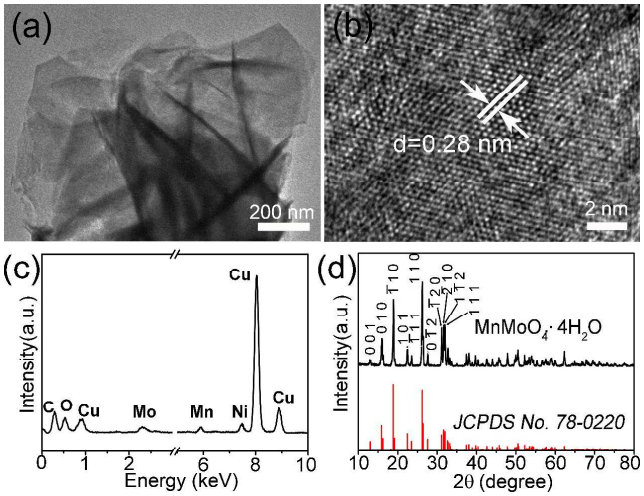

Fig. 2 (a) TEM image of $MnMoO_4$•$4H_2O$ NPs. (b) High-resolution TEM image of a $MnMoO_4$•$4H_2O$ NP. (c) EDS pattern of $MnMoO_4$•$4H_2O$ NPs. (d) Typical XRD pattern of $MnMoO_4$•$4H_2O$ NPs scratched from the Ni foam.

Transmission electron microscopy (TEM) was used to further investigate the structure of the as-obtained $MnMoO_4$•$4H_2O$ NPs. Fig. 2(a) depicts typical TEM image of $MnMoO_4$•$4H_2O$ NPs after strong ultrasonic vibration in ethanol. The representative high-resolution TEM image of $MnMoO_4$•$4H_2O$ NPs shown in Fig. 2(b) clearly reveals interplanar spacing of 0.28 nm, corresponding to the (111) plane. The elemental spatial distributions across the $MnMoO_4$•$4H_2O$ NPs were characterized by energy dispersive spectroscopy (EDS), revealing the presence of elements of Mn, Mo, and O, as shown in Fig. 2(c). The crystal phase of the $MnMoO_4$•$4H_2O$ NPs was examined by XRD. In order to avoid the effect of the Ni foam substrate on the XRD peak signals, the powder of the products gently scratched from the Ni foam was used for XRD analysis. As indicated in Fig. 2(d), the XRD pattern is well in accordance with the standard diffraction pattern of $MnMoO_4$•$4H_2O$. All the typical diffraction peaks are observed to correspond well to those of the standard pattern.

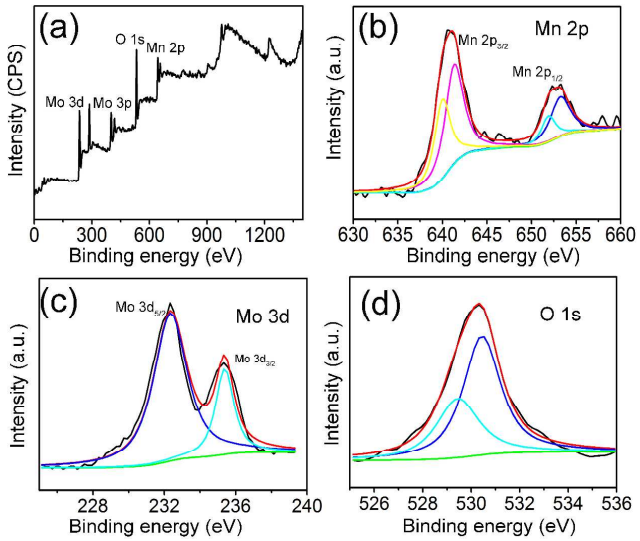

Fig. 3 (a) XPS survey spectrum. (b) Mn 2p core level spectrum. (c) Mo 3d core level spectrum. (d) O 1s core level spectrum of $MnMoO_4$•$4H_2O$.

XPS survey spectrum was conducted to explore the composition of as-prepared $MnMoO_4$•$4H_2O$ sample. The wide scan surface survey of the sample was shown in Fig. 3(a), displaying three peaks situated at 640.8 eV, 530.3 eV and 232.4 eV, indicating Mn 2p, O 1s, and Mo 3d levels, respectively. Fig. 3(b) represents the Mn 2p core level spectrum, which can be deconvoluted into four peaks. The binding energy peak at 641.3 eV corresponds to Mn $2p_{3/2}$, whereas, the binding energy peak at 652.9 eV corresponds to the Mn $2p_{1/2}$ level. The main binding energy peaks of Mn $2p_{3/2}$ and Mn $2p_{1/2}$ are separated by 11.6 eV, which is a signature of the Mn^{2+} oxidation state.[9,32] The Mo 3d core level spectrum (Fig. 3(c)) shows two peaks with binding energies of 232.1 eV and 235.3 eV, corresponding to Mo $3d_{5/2}$ and Mo $3d_{3/2}$, respectively. The binding energy peak of Mo 3d is separated by 3.2 eV, which also signifies a Mo^{6+} oxidation state.[33] The O 1s core level spectrum (Fig. 3(d)) contains two peaks at binding energies of 529.3 eV and 530.3 eV, representing the O 1s level in $MnMoO_4$•$4H_2O$.[34]

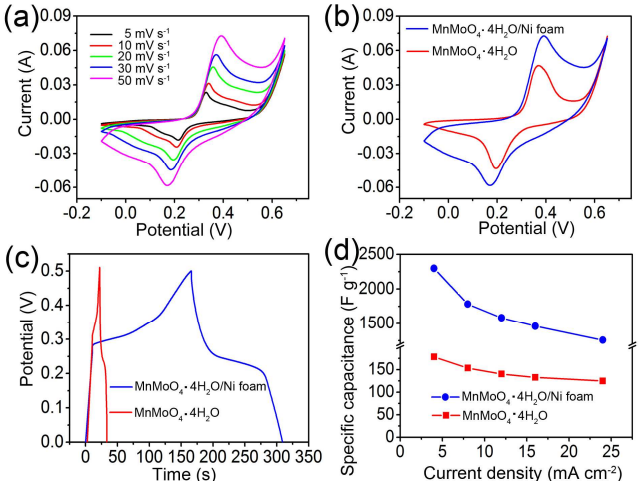

Fig. 4 (a) CV curves of the $MnMoO_4$•$4H_2O$ NPs at various scan rates. (b) A comparison of CV curves of $MnMoO_4$•$4H_2O$ NPs on the Ni foam and $MnMoO_4$•$4H_2O$ powder at a scan rate of 50 mV s^{-1}. (c) A comparison of Galvanostatic charge-discharge curves of $MnMoO_4$•$4H_2O$ NPs on Ni foam and $MnMoO_4$•$4H_2O$ powder electrode at discharge current densities

of 4 mA cm^{-2}. (d) A comparison of specific capacitances for $MnMoO_4•4H_2O$ NPs on Ni foam and $MnMoO_4•4H_2O$ powder as a function of current density.

In order to explore the electrochemical properties of the $MnMoO_4•4H_2O$ NPs on Ni foam and $MnMoO_4•4H_2O$ powder (Fig. S1, see ESI†), both cyclic voltammetry (CV) and galvanostatic charge-discharge (CD) cycling measurement were carried out with 1 M NaOH aqueous solution in a three-electrode system. Fig. 4(a) shows the CV curves of the $MnMoO_4•4H_2O$ NPs electrode within the potential range of -0.1 to 0.65 V at various sweeping rates ranging from 5 mV s^{-1} to 50 mV s^{-1}. Obviously, a pair of distinct redox peaks is visible in each CV curves demonstrating that the capacitance characteristics are mainly ascribed to the Faradic capacitive behavior. The anodic peak is related to the oxidation process, and the cathodic peak is connected with reduction process. With the increase of scan rates, the shapes of the CV curves at different scan rates do not change and the peaks of CV curves positions change. The anodic peaks gradually shift to higher potentials, but the cathodic peaks change in the opposite direction. These indicated that at higher scan rates the electronic and ionic transportation are rapid and electroactive material/electrolyte interface occurs the fast redox reactions. According to the CV curves the $MnMoO_4•4H_2O$ NPs supported on Ni foam exhibited wonderful pseudocapacitor behaviours with area specific capacity of 1.03 F cm^{-2} (specific capacitance value 2060 F g^{-1}) at a scan rate of 5 mV s^{-1}. The CV curves with $MnMoO_4•4H_2O$ NPs on Ni foam and pure $MnMoO_4•4H_2O$ powder at scan rate of 50 mV s^{-1} were displayed at Fig. 4(b). It is evident that the CV integrated area of the $MnMoO_4•4H_2O$ NPs electrode materials on Ni foam is apparently larger than that of the pure $MnMoO_4•4H_2O$ powder electrode material, indicating that the $MnMoO_4•4H_2O$ NPs electrode material on the Ni foam has a significantly larger specific capacitance than pure $MnMoO_4•4H_2O$ powder electrode material (Fig. S2, see ESI†). Galvanostatic charge-discharge measurements performed at different current densities were employed to further confirm such an improved electrochemical performance of the $MnMoO_4•4H_2O$ NPs electrode materials on Ni foam. Fig. 4(c) depicts the comparison of CD curves at a stable potential window between 0 and 0.5 V for the $MnMoO_4•4H_2O$ NPs on Ni foam and $MnMoO_4•4H_2O$ powder electrodes at the same current density of 4 mA cm^{-2}. As shown in Fig. 4 (c), the electrode material of the $MnMoO_4•4H_2O$ nanoplates on the Ni foam reveals a much longer discharging time compared with that of $MnMoO_4•4H_2O$ powders. It means the $MnMoO_4•4H_2O$ NPs electrode material on Ni foam demonstrates higher specific capacitance values than the pure $MnMoO_4•4H_2O$ powder electrode material. Fig. 4(d) displays typical results of CD curves for the $MnMoO_4•4H_2O$ NPs on the Ni foam (Fig. S3, see ESI†) and pure $MnMoO_4•4H_2O$ powder electrodes within current densities range from 4 to 24 mA cm^{-2}. The area specific capacitance values of the $MnMoO_4•4H_2O$ NPs were calculated from the discharge time, ranging from 1.15, 0.89, 0.79, 0.73, and 0.63 F cm^{-2} (specific capacitance values of 2300, 1780, 1580, 1460, and 1260 F g^{-1}) at current densities of 4, 8, 12, 16, and 24 mA cm^{-2}, respectively. The values of capacitors gradually dropped from 1.15 F cm^{-2} (specific capacitance of 2300 F g^{-1}) at a current density of 4 mA cm^{-2} to 1.15 F cm^{-2} (specific capacitance of 1260 F g^{-1}) at a current density of 24 mA cm^{-2}.

These drops may be ascribed to the incremental voltage drop and insufficient active material involved in redox reaction with the increase of current density. However, even at a higher current density, the $MnMoO_4•4H_2O$ NPs still shows a high capacitance, nearly 54.8% of the initial capacitance remaining. Such high area specific capacitance at large current densities further proves the great advantages of the $MnMoO_4•4H_2O$ NPs. But the pure $MnMoO_4•4H_2O$ powder only shows area specific capacitance of 0.36 F cm^{-2} (178F g^{-1}) at 4 mA cm^{-2}, much less than the $MnMoO_4•4H_2O$ NPs electrode materials on Ni foam. The superior electrochemical performances of the $MnMoO_4•4H_2O$ NPs are mainly attributed to the advantageous structure of the electrode. The thin NPs give rise to a high surface area, providing more active reaction sites and improving the utilization of active materials.[35] Besides, the large open space between the NPs can greatly enhance the kinetics of ion and electron transport inside the electrodes.[36] The unique porous structure of $MnMoO_4•4H_2O$ NPs on Ni foam provides more active sites for efficient electrolyte ions transportation not only on the active material surface but also throughout the bulk.

Furthermore, the specific capacitance reported here is much higher than those reported for $MnMoO_4$ base materials, such as α-$MnMoO_4$ nanorods (998 F g^{-1} at 5mV s^{-1}),[25] $MnMoO_4$/$CoMoO_4$ heterostructured nanowires (187.1 F g^{-1} at 1 A g^{-1}),[26] and is even higher than those previously reported $CoMoO_4$ and $NiMoO_4$ pseudocapacitive materials, such as $CoMoO_4•0.9H_2O$ nanorods (326 F g^{-1} at 5 mA cm^{-2}),[37] $CoMoO_4$ nanorods (286 F g^{-1} at 5mA cm^{-2}),[38] α-$NiMoO_4$ (1517 F g^{-1} at 1.2 A g^{-1}),[39] etc.

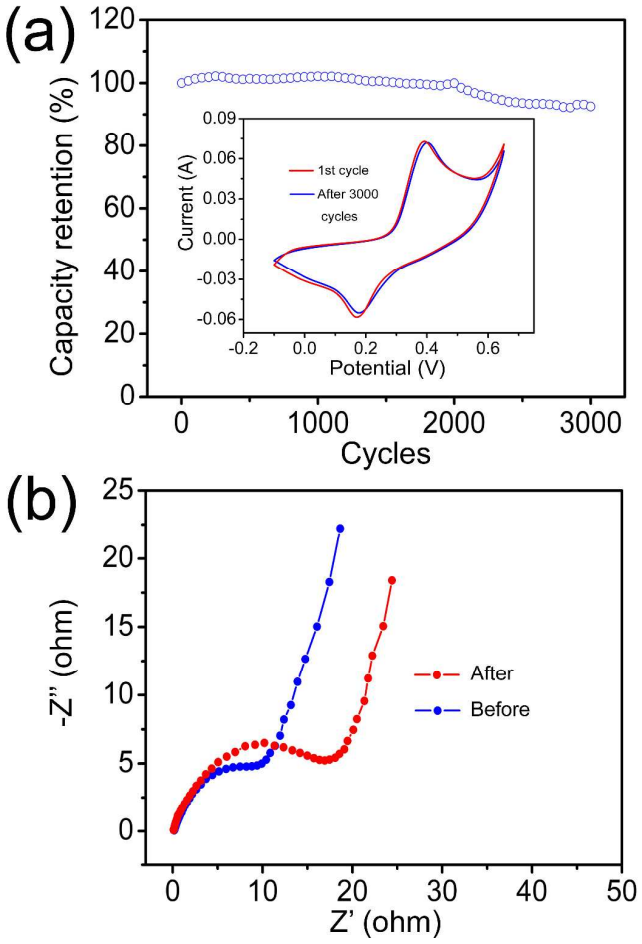

Fig. 5 (a) Cycling performance of $MnMoO_4$•$4H_2O$ NPs grown on Ni foam at a scan rate of 5 mV s^{-1} and (inset) the 1st and 3000th cycles of CV profiles at a scan rate of 5 mV s^{-1}. (b) Electrochemical impedance spectra before and after cycling.

The durability of the electrode materials is a critical aspect for practical applications. The cycling performance was conducted in the range of 0-0.65 V in 1 M NaOH aqueous solution. Fig. 5(a) characterizes cycling performance of 3000 cycles. There is still approximately 92% retention of its initial capacitance after 3000 cycles. The capacitance retention of the $MnMoO_4$•$4H_2O$ NPs on the Ni foam is better than other reported results, such as ZnO@Ni_3S_2 nanowires (42% capacitance retention after 2000 cycles at 10 A g^{-1}),[40] Co3O4@$Ni(OH)_2$ nanowires (76% capacitance retention after 1000 cycles at 50 mA cm^{-2}). [41] Thus the unique $MnMoO_4$•$4H_2O$ NPs electrode displays high electrochemical stability for long cycle life applications. There is a knee point at about 2000 cycle on the cycling performance curve in Fig. 5(a). It can be ascribed to a minor damage of the $MnMoO_4$•$4H_2O$ NPs electrode active materials after experiencing harsh and frequent phase variations during the redox reactions and destruction/reconstruction of the structures, leading capacity change.[42,43] Although at about 2000 cycles the capacitance changes obviously, gradually falling after this knee point, and 92% capacitance retention after 3000 cycles indicates that a minimal collapse and disassembly of the $MnMoO_4$•$4H_2O$ NPs electrode materials occur and the mechanical structure of the electrode materials hasn't been broken. Fig. 5 (a) inset shows the 1st and the 3000th CV curves of charge-discharge cycling tests at a scan rate of 50 mV s^{-1}. After 3000 cycles the CV curve shape almost has no change compared with the 1st cycling curve, indicating stable electrochemical properties of the active material. The directly growing nanomaterials on the Ni foam ensure good electrical conductivity and strong mechanical adhesion to the underneath conductive Ni foam substrate, avoiding a binder which commonly adds dead weight and extra contact resistance and building fast electron-transport access.

The resulting Nyquist plots were pictured in Fig. 5 (b) including an arc in the middle- and high-frequency region and a sloped line in the low-frequency region. The two spectra exhibited obvious differences before and after 3000 cycles. A careful observation shows that the radius of the semicircle for 1st cycle was slightly smaller than 3000th cycle in the high-frequency region suggesting a slight decline tendency of the interfacial charge transfer conductivity of $MnMoO_4$•$4H_2O$ NPs electrode. Besides, at lower frequencies, the diffusive resistance (Warburg impedance) of $MnMoO_4$•$4H_2O$ NPs electrode slightly increased after 3000 cycles and the slope of the straight line in the low frequency region is still larger than that of 45° straight line, showing that the electrolyte penetration and ion diffusion in the host materials have not reduced notably. Impedance spectra of the $MnMoO_4$•$4H_2O$ NPs were conducted to further understand the change of this electrode material device after 3000 cycles. Worthwhile structural and electrochemical information could be obtained by analyzing morphology of the electrodes tested after many cycles. After long-term cycling, the colour of electrolyte demonstrated no visible changes and the $MnMoO_4$•$4H_2O$ NPs nanostructures have not changed obviously, as is displayed by SEM characterization in Fig. S4(see ESI†). This reveals that the structure and electrochemistry are stable during the cycling. These results can indicate that the $MnMoO_4$•$4H_2O$ NPs material is a desirable supercapacitor electrode material.

4. Conclusions

A facile one-pot hydrothermal process was developed to synthesize the $MnMoO_4$•$4H_2O$ NPs on the Ni foam with high electrochemical properties as supercapacitor electrode. The as-synthesed $MnMoO_4$•$4H_2O$ NPs electrode on Ni foam demonstrated excellent electrochemical performances, i.e., a high capacitance of 1.15 F cm^{-2} (2300 F g^{-1}) at a current density of 4 mA cm^{-2}, desirable rate property and cycling stability. The high electrochemical behaviors can be attributed to the NPs interconnected porous structure and synergistic effects between both manganese and molybdenum ions in binary oxide. Furthermore, the $MnMoO_4$•$4H_2O$ NPs directly grown on the Ni foam greatly improved electrochemical capabilities compared to the $MnMoO_4$•$4H_2O$ powder. It is expected that in terms of their outstanding intrinsic electrochemical capacitance properties, the $MnMoO_4$•$4H_2O$ NPs are a promising material for application in supercapacitors.

Acknowledgements

This work was financially supported by the National Natural Science Foundation of China (Grant No. 21171035 and 51272299), the Key Grant Project of Chinese Ministry of Education (Grant No. 313015), the Scientific Research

Foundation for the Returned Overseas Chinese Scholars, the Science and Technology Commission of Shanghai-based "Innovation Action Plan" Project (Grant No. 10JC1400100), Shanghai Rising-Star Program (Grant No. 11QA1400100), Innovation Program of Shanghai Municipal Education Commission (Grant No. 13ZZ053), Shanghai Leading Academic Discipline Project (Grant No. B603), Ph.D. Programs Foundation of Ministry of Education of China (Grant No. 20110075110008), the Fundamental Research Funds for the Central Universities, and the Program of Introducing Talents of Discipline to Universities (Grant No. 111-2-04). the State Key Laboratory for Modification of Chemical Fibers and Polymer Materials (Grant No. LK1218), Donghua University.

Notes and references

[a]*State Key Laboratory for Modification of Chemical Fibers and Polymer Materials, College of Materials Science and Engineering, Donghua University, Shanghai 201620, China.*
[b]*School of Fundamental Studies, Shanghai University of Engineering Science, Shanghai 201620, China*
Fax: +86-21-6779-2947; Tel: +86-21-6779-2947; E-mail: yangjm@dhu.edu.cn; phqin@dhu.edu.cn;hu.junqing@dhu.edu.cn;
† Electronic Supplementary Information (ESI) available: [Experimental process, Supplementary Fig.s and Specific capacitance calculation]. See DOI: 10.1039/b000000x/

1 P. Simon and Y. Gogotsi, *Nat. Mater.*, 2008, **7**, 845.
2 J. R. Miller and P. Simon, *Science*, 2008, **321**, 651.
3 D. Pech, M. Brunet, H. Durou, P. Huang, V. Mochalin and Y. Gogotsi, *Nat. Nanotechnol.*, 2010, **5**, 651.
4 M.Winter, R. J.Brodd, *Chem. Rev.*, 2004, **104**, 4245.
5 D. Liu, Q. F. Zhang, P. Xiao, B. B. Garcia, Q. Guo, R. Champion, G.Z. Cao, *Chem. Mater.*, 2008, **20**, 1376.
6 Y. Zhang, H. Feng, X. Wu, L. Wang, A. Zhang, T. Xia, H. Dong, X. Li, L. Zhang, *Int. J. Hydrogen Energ.*, 2009 , **34**, 4889.
7 J. Jiang,Y. Li, J. Liu, X. Huang, C. Yuan, X. W. Lou, *Adv. Mater.*, 2012, **24**, 5166.
8 X. Zhang, D. D. Zhao, Y. Q. Zhao, P. Y. Tang, Y. L. Shen, C. L. Xu, H. L. Lia and Y. Xiao, *J. Mater. Chem. A*, 2013, **1**, 3706.
9 S. S. Wu, W. F. Chen and L. F. Yan, *J. Mater. Chem. A*, 2014, **2**, 2765.
10 H. W. Wang, H. Yi, X. Chen and X. F. Wang, *J. Mater. Chem. A*, 2014, **2**, 3223.
11 Q. Lu, M. W. Lattanzi, Y. Chen, X. Kou, W. Li, X. Fan, K. M. Unruh, J. G. Chen and J. Q. Xiao, *Angew. Chem.*, 2011, **123**, 6979.
12 C. Z. Yuan, L. Yang, L. R. Hou, L. F. Shen, X. G. Zhang and X. W. Lou, *Energy Environ. Sci.*, 2012, **5**, 7883.
13 X. H. Lu, T. Zhai, X. H. Zhan, Y. Q. Shen, L. Y. Yuan, B. Hu, L. Gong, J. Chen, J. Zhou, Y. X. Tong and Z. L. Wang, *Adv. Mater.*, 2012, **24**, 938.
14 K. V. Sankar and R. K. Selvan, *RSC Adv.*, 2014, **4**, 17555.
15 X. H. Lu, X. Huang, S. L. Xie, T. Zhai, C. S. Wang, P. Zhang, M. H. Yu, W. Li, C. L. Liang and Y. X. Tong, *J. Mater. Chem.*, 2012, **22**, 13357.
16 K. Karthikeyan, D. Kalpana, N. G. Renganathan, *Ionics*, 2009, **15**, 107.
17 L. Bao, J. Zang, X. Li, *Nano Lett.*, 2011, **11**, 1215.
18 M. C. Liu, L. B. Kong, C. Lu, X. J. Ma, X. M. Li, Y. C. Luo, L. Kang, *J. Mater. Chem. A*, 2013, **1**, 1380.
19 X. Z. Yu, B. Lu, and Z. Xu, *Adv. Mater.*, 2014, **26**, 1044.
20 X. Xia, W. Lei, Q. Hao, W. Wang and X. Wang, *Electrochim. Acta*, 2013, **99**, 253.
21 Q. F. Wang, B. Liu, X. F. Wang, S. H. Ran, L. M. Wang, D. Chen and G. Z. Shen, *J. Mater. Chem.*, 2012, **22**, 21647.
22 Q. F. Wang, X. F. Wang, J. Xu, X. Ouyang, X. J. Hou, D. Chen, R. M. Wang, G. Z. Shen, *Nano Energy*, 2014, **8**, 44.
23 B. Liu, D. S. Tan, X. F. Wang, D. Chen, and G. Z. Shen, *Small*, 2013, **9**, 1998.
24 Q. F. Wang, J. Xu, X. F. Wang, B. Liu, X. J. Hou, G. Yu, P. Wang, D. Chen, and G. Z. Shen, *ChemElectroChem*, 2014, **1**, 559.
25 K. K. Purushothaman, M. Cuba and G. Muralidharan, *Mater. Res. Bull.*, 2012, **47**, 3348.
26 L. Q. Mai, F. Yang, Y. L. Zhao, X. Xu, L. Xu and Y. Z. Luo, *Nat.Commun.*, 2011, **2**, 381.
27 Z. W. Xu, Z. Li, X. H. Tan, C. M. B. Holt, L. Zhang, B. S. Amirkhiz and D. Mitlin, *RSC Adv.*, 2012, **2**, 2753.
28 D. Guo, P. Zhang, H. M. Zhang, X. Z. Yu, J. Zhu, Q. H. Li and T. H. Wang, *J. Mater. Chem. A*, 2013, **1**, 9024.
29 D. Guo, H. M. Zhang, X. Z. Yu, M. Zhang, P. Zhang, Q. H. Li and T. H. Wang, *J. Mater. Chem. A*, 2013, **1**, 7247.
30 H. N. Zhang, Y. J. Chen, W. W. Wang, G. H. Zhang, M. Zhuo, H. M. Zhang, T. Yang, Q. H. Li and T. H. Wang, *J. Mater. Chem. A*, 2013, **1**, 8593.
31 Q. F. Wang, X. F. Wang, B. Liu, G. Yu, X. J. Hou, D.Chen and G. Z. Shen, *J. Mater. Chem. A*, 2013, **1**, 2468.
32 H. C. Gao, F. Xiao, C. B. Ching and H. W. Duan, *ACS Appl. Mater. Interfaces*, 2012, **4**, 2801.
33 X. Xia, W. Lei, Q. Hao, W. Wang and X. Wang, *Electrochim. Acta*, 2013, **99**, 253.
34 J. Haetge, I. Djerdj and T. Brezesinski, *Chem. Commun.*, 2012, **48**, 6726.
35 R. N. Singh,M.Hamdani, J. F. Koenig, G. Poillerat, J. L. Gautier and P. Chartier, *J. Appl. Electrochem.*, 1990, **20**, 442.
36 X. H. Xia, J. P. Tu, Y. Q. Zhang, Y. J. Mai, X. L. Wang, C. D. Gu and X. B. Zhao, *RSC Adv.*, 2012, **2**, 1835.
37 M. C. Liu, L. B. Kong, X. J. Ma, C. Lu, X. M. Li, Y. C. Luo and L. Kang, *New J. Chem.*, 2012, **36**, 1713.
38 C. Z. Yuan, L. Yang, L. R. Hou, J. Y. Li, Y. X. Sun, X. G. Zhang, L. F. Shen, X. J. Lu, S. L. Xiong and X. W. Lou, *Adv. Funct. Mater.*, 2012, **22**, 2560.
39 B. Senthilkumar, K. V. Sankar, R. K. Selvan, M. Danielleb and M. Manickamb, *RSC Adv.*, 2013, **3**, 352.
40 Z. Xing, Q. Chu, X. Ren, C. Ge, A. H. Qusti, A. M. Asiri, A. O. Alyoubi, X. Sun, *J. Power Sources*, 2014, 245, 463.
41 C. H. Tang, X. Yin, H. Gong, *ACS Appl. Mater. Interfaces*, 2013, 5, 10574.
42 C. Zhou, Y. W. Zhang, Y. Y. Li and J. P. Liu, *Nano Lett.*, 2013, 13, 2078.
43 B. Saravanakumar, K. K. Purushothaman and G. Muralidharan, *ACS Appl. Mater. Interfaces*, 2012, 4, 4484.

The table of contents entry

The $MnMoO_4$•$4H_2O$ nanoplates were directly grown on a Ni foam by a facile hydrothermal route with enhanced electrochemical performances, i.e., a high specific capacitance of 1.15 F cm^{-2} (2300 F g^{-1}) at 4 mA cm^{-2} and a good cycling stability of 92% of the initial specific capacitance after 3000 cycles, which may be considered as a perspective material for high-performance electrochemical capacitors.